

Hydrogen Production from Ethanol Steam Reforming over SnO₂-K₂O/Zeolite Y Catalyst

Jun Sung Lee, Jieun Kim, and Misook Kang*

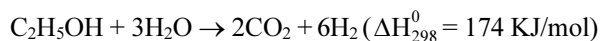
Department of Chemistry, College of Science, Yeungnam University, Gyeongbuk 712-749, Korea. *E-mail: mskang@ynu.ac.kr
Received February 17, 2011, Accepted April 19, 2011

The SnO₂ with a particle size of about 300 nm instead of Ni is used in this study to overcome rapid catalytic deactivation by the formation of a NiAl₂O₄ spinel structure on the conventional Ni/ γ -Al₂O₃ catalyst and simultaneously impregnated the catalyst with potassium (K). The SnO₂-K₂O impregnated Zeolite Y catalyst (SnO₂-K₂O/ZY) exhibited significantly higher ethanol reforming reactivity than that achieved with SnO₂ 100 and SnO₂ 30 wt %/ZY catalysts. The main products from ethanol steam reforming (ESR) over the SnO₂-K₂O/ZY catalyst were H₂, CO₂, and CH₄, with no evidence of any CO molecule formation. The H₂ production and ethanol conversion were maximized at 89% and 100%, respectively, over SnO₂ 30 wt %-K₂O 3.0 wt %/ZY at 600 °C for 1 h at a CH₃CH₂OH:H₂O ratio of 1:1 and a gas hourly space velocity (GHSV) of 12,700 h⁻¹. No catalytic deactivation occurred for up to 73 h. This result is attributable to the easier and weaker reduction of Sn components and acidities over SnO₂-K₂O/ZY catalyst, respectively, than those of Ni/ γ -Al₂O₃ catalysts.

Key Words : Hydrogen production, Ethanol steam-reforming reaction, SnO₂ 30 wt %/ZY, SnO₂ 30 wt %-K₂O 3.0 wt %/ZY

Introduction

Recently, ethanol has been used for steam reforming (SR) to produce hydrogen because of its non-toxicity and ease of transport and storage. The oxidation temperature of ethanol is higher than that of methanol or dimethyl ether, rendering difficult its decomposition. However, one advantage of this method is that more hydrogen can be produced per mole of ethanol that is reformed because hydrogen can also be extracted from the steam according to the following equation.^{1,2}



On the other hand, nickel-based catalysts that were supported on Al₂O₃, SiO₂, and various zeolites containing alkali metals have been investigated for the ethanol-reforming reactions.³⁻⁷ However, the coke formation that occurs through the rapid sintering between the Ni and Al₂O₃ supports is a serious problem.^{8,9} Under SR conditions, the intermediates to CO and H₂, and the adsorbed CH_x species on the Ni surface can undergo further dehydrogenation, polymerization, and rearrangement into highly stable carbon species that not only show low reactivity toward the gasification reaction, but also rapid catalytic deactivation. An especially serious problem in NiAl₂O₄ catalysts is the abrupt catalytic deactivation that occurs at high temperatures above 650 °C, due to the formation of a NiAl₂O₄ spinel structure resulting from the strong sintering between Ni and Al, and this deactivation leads to reactor shutdown and the reversal of the feed gases.^{8,9} To depress the strong sintering affection between Ni and Al, activated noble metals such as Pt or Pd have recently been coated on the surface of some support. Aksoylu *et al.*¹⁰ reported that the Pt-Ni catalyst was very prone to catalytic deactivation at low steam/CO ratios accompanied by high

C/O₂ ratios. However, some problems remain in terms of the catalytic activity and lifetime. Additionally the hydrogen evolution was shifted to a higher temperature over some catalysts with these novel metals, Pd and Pt,^{11,12} which are, furthermore, very expensive. Therefore the amount of precious metal catalyst that is required is an important issue for the commercialization of ethanol reforming. A new trend involves the exclusion of the nickel content. Víctor A. de la Peña O'Shea *et al.*¹³ reported on the Fe-promoter effect over Co-based catalysts for the selective H₂-production by ethanol SR (ESR). Their catalytic activity depended on the iron content. The catalytic performance was enhanced and the production of undesired CO and CH₄ by-products was decreased for the catalyst derived from Fe_{0.15}Co_{2.85}O₄. After 50 h of reaction, an ethanol feed of 5.9 mol H₂/mol was obtained. In another examination of hydrogen production from the SR of ethanol and glycerol over ceria-supported metal catalysts, Baocai Zhang *et al.*¹⁴ reported that CeO₂-supported Ir, Co and Ni catalysts are significantly active and selective for hydrogen production from the SR reactions of ethanol and glycerol. Particularly, the Ir/CeO₂ catalyst showed promising catalytic performance for both reactions. Therefore, like previous researchers, we excluded nickel-containing catalysts from our investigation of the ESR reaction. We suggest that the presence of a metal component with a capability for ethanol cracking by donating electrons will improve the hydrogen production in ESR. Therefore, we introduced SnO₂, which has high electron transfer ability even at high temperature, onto the Zeolite Y support. SnO₂ is widely used as battery, semiconductor, and superconductor materials.¹⁵⁻¹⁷ The degradation of the catalyst possibly supports the conversion to methyl groups of various intermediates over the Sn component, because of its reverse

hydrogen or electron spillover property and the dehydrogenation of ethanol. Additionally, we expect the impregnated K component to simultaneously reduce the extent of catalytic deactivation caused by the partial sintering between the Sn and the Al component in the Zeolite Y support during ESR, and to depress the strong acidity of the Zeolite Y catalyst.

Experimental

Preparation of the Three Catalysts, SnO₂ 100 wt %, SnO₂ 30 wt %/ZY, and SnO₂ 30 wt %-K₂O 3.0 wt %/ZY. To find the most suitable catalyst, various amounts of SnO₂, 10, 20, 30, 50, and 100 wt % over Zeolite Y support was impregnated and conducted ethanol steam reforming. As a result, the best performance for H₂ evolution showed over 30 wt % SnO₂/ZY, and it was decreased 20, 10, 50, 100 wt % in order. Furthermore, an alkaline ingredient, 1.0, 3.0, 5.0 and 10.0 wt % of K₂O was simultaneously added for the durability and suppressing the presence of Al, and the results of hydrogen production was the best on 3.0 wt % of K₂O catalyst. On the basis of the above, the three catalysts, SnO₂ 100 wt %, SnO₂ 30 wt %/ZY, and SnO₂ 30 wt %-K₂O 3.0 wt %/ZY, were selected and prepared by conventional impregnation method. First, SnO₂ particles were prepared by a hydrothermal method. As a Sn source, SnCl₂ (99.99%, Junsei com., Japan) was dissolved in water and the slurry pH was fixed at 10.0 for rapid hydrolysis. The slurry was homogeneously stirred for 2 h, transferred to an autoclave, and thermally treated at 200 °C for 24 h in a nitrogen environment. After thermal reaction, the attained SnO₂ powder was washed until the pH was neutralized at 7, dried at 80 °C for 24 h in air condition, and finally calcined at 500 °C for 3 h in O₂ condition. For SnO₂-K₂O/ZY, 1.0 g of Zeolite Y (ZY, 0.8-1.5 μm, 680 m²/g) was impregnated with a mixture 30 wt % SnO₂ (30 wt % as-synthesized here, 300 nm) and 5.0 wt % KOH (Junsei Co., Japan; calculated to be about 3.0 wt % K₂O) in 25 mL of ethanol. The slurry was stirred for 10 h, evaporated at 60-70 °C for 3 h, and then calcined at 500 °C for 2 h in air. For comparison, SnO₂/ZY was also prepared in the same way. The three catalysts were reduced with H₂ at 700 °C for 2 h, and then cooled to room temperature under argon gas.

Characterizations of the Three Catalysts and Ethanol Steam-Reforming (ESR) Reaction. The three prepared catalysts were identified through powder XRD (MPD model, PANalytical, Yeungnam University Instrumental Analysis Center, Korea) analysis with nickel-filtered Cu Kα radiation (30 kV, 30 mA). The particle shapes of the three catalysts were determined by field emission scanning electron microscopy (FESEM; S-4100, Hitachi, Yeungnam University Instrumental Analysis Center, Korea) operated at 120 kV. The Brunauer, Emmett and Teller (BET) surface area was measured using a Micrometrics ASAP 2000 instrument. XPS measurements of the Sn3d, Si2p, Al2p, K2p, and C1s orbitals were recorded with a model AXIS-NOVA (Kratos Inc., Korea Basic Science Institute Jeonju Center, Korea)

system, equipped with a non-monochromatic AlKα (1486.6 eV) X-ray source. NH₃-TPD measurements were carried out on a conventional TPD system using an N-1000 thermogravimetric analyzer (TGA; Scinco, Korea). The change in the hydrogen concentration was measured with a gas chromatograph (GC series 580, GOW-MAC) equipped with a thermal conductivity detector (TCD). In order to study the formation of carbon species on the catalyst surface, temperature-programmed oxidation (TPO) was performed using the TGA N-1000 instrument by introducing high purity oxygen gas into the system after N₂ purging. The reactor for the ESR is the same to that in previous our report.¹⁸ The catalytic activities were measured in the temperature range of 200-800 °C for 1 h reaction time intervals at steam-to-ethanol ratios of 1:1, 1:2, and 1:3, with gas hourly space velocity (GHSV) of 3175, 6350, and 12,700 h⁻¹. The catalyst (0.4 g) was pelletized to 20-25 mesh and then packed with a small amount of quartz wool to prevent its movement in the fixed-bed quartz reactor, which was vertically mounted inside the furnace. First, all of the catalysts were reduced in situ under hydrogen (10 mL/min) for 2 h at 700 °C prior to each run. An ethanol/water solution (mol/mol) was then introduced into the vaporizer. In this study, the amount of steam was adjusted by regulating the temperature, according to the following partial pressure law: $\ln P_1/P_2 = -\Delta H/R (1/T_1 - 1/T_2)$

Here, P₁, P₂, T₁, T₂, H, and R correspond to the pressure at 760 mmHg, the pressure at an arbitrary boiling point, the temperature (in Kelvin) at P₁, the temperature (in Kelvin) at P₂, the enthalpy, and the gas constant (8.3145 kPa·dm³/mol·K), respectively. First, the enthalpy was obtained at all of the known, two-point pressures, and then the pressure (P₁, mmHg) was calculated corresponding to the arbitrary volume (or mol) %. Finally, the temperature T₁ was determined. The vaporization temperatures were affected by the ethanol and steam concentrations. Based on this equation, ethanol and water were vaporized at 24 °C and 30 °C, respectively, which corresponded to 30 wt %/Ar carrier gases. The ethanol to steam ratio was regulated by each flow meter, and the total flow rate was held constant at 50 mL/min for both ethanol and steam. The GHSV was calculated based on the total flow rate of the feed mixture in the gas phase. The reaction products were measured using on-line GC on a Donam DS6200 (Donam company, Korea) equipped with a TCD and a flame ionizing detector (FID), used respectively to detect H₂, CH₃CHO, C₂H₅OH, CO, and CO₂, and CH₄, C₂-C₅ hydrocarbons and other products. The ethanol conversion (X_{EtOH}) and the selectivity of the C-containing products (SC) of the various samples were calculated using the following equations:

$$X_{\text{EtOH}} = (\text{mol EtOH}_{\text{in}} - \text{mol EtOH}_{\text{out}}) / \text{mol EtOH}_{\text{in}} \times 100\%$$

$$SC_{\text{H}_2} = \text{mol H}_2 / [(\text{mol EtOH}_{\text{in}} - \text{mol EtOH}_{\text{out}}) - (\text{mol H}_2\text{O}_{\text{in}} - \text{mol H}_2\text{O}_{\text{out}})] \times 100\%$$

$$SC_{\text{others}} = \text{mol others}_{\text{out}} / (\text{mol EtOH}_{\text{in}} - \text{mol EtOH}_{\text{out}}) \times 100\%$$

Results and Discussion

Characteristics of the Three Catalysts. The three catalysts, both pre-treated and untreated by H₂ gas at 700 °C before the reaction, were characterized on the basis of the XRD patterns shown in Figure 1. The special peaks of Zeolite Y,¹⁹ acting as the catalyst support, were observed at 2-theta angles of 32, 23, and 7° in two samples: SnO₂ 30 wt %/ZY and SnO₂ 30 wt %-K₂O 3.0 wt %/ZY. Almost all of the diffraction lines of the SnO₂ phase²⁰ at 2-theta angles of around 26, 34, 37, 52, 54, 57, 62, 64, 66, 72, and 78° could be seen in the XRD patterns of all three catalysts, and the peaks were largely unaffected, although slightly decreased, by the H₂ reduction. Scherrer's equation,²¹ $t = 0.9\lambda/\beta\cos\theta$, where λ is the wavelength of the incident X-rays, β the full width at half maximum (FWHM) height in radians, and θ the diffraction angle, was used to estimate the crystalline domain size. When the FWHM of the peak at 34° 2 θ was selected in SnO₂, the calculated crystalline domain size was 255 nm. On the other hand, the peak assigned to K₂O was not seen either before or after the H₂ reduction, because it was below the detection limit. The three catalysts were characterized using the FESEM images in Figure 2. The images of the pure SnO₂ and Zeolite Y exhibited regular spherical and hexagonal morphologies with an average particle size of 200-250 nm and 0.7-1.2 μ m, respectively. The SnO₂ particles in the SnO₂/ZY catalyst appeared to be well dispersed on the surface of Zeolite Y. However, new grains were grown between Sn and K in SnO₂-K₂O/ZY, implying that the co-existence of the Sn and K components rendered the crystals rather uniform compared to those of the catalysts containing only Sn component. The surface

areas were slightly depressed by the Sn and K loading on the Zeolite Y, 462 m²/g in SnO₂-K₂O/ZY, which was attributed to the partial covering of the Sn and K on pore spaces of Zeolite Y particles. To determine the relation between the catalytic performance and the Brønsted acidic properties, the NH₃-TPD profiles of the three catalysts were obtained and are shown in Figure 3. Solid catalytic materials possess many acid sites and certain acidic strengths that are attributed to their high Al contents and tetrahedral Al sites, respectively. A broad peak around 100-200 °C was attributed in this study to the presence of Al in Zeolite Y. The reactions of ethanol reforming, ethanol oxidation by oxygen from the injected water, and reduction of carbon oxides in the former and of hydrocarbons by proton ions at the Brønsted acid sites all occur simultaneously. The latter reaction affects the absolute performance of the catalyst. Consequently, the number of acid sites and their strength are both important. In general, the NH₃-TPD profiles of the porous catalysts consist of two peaks: one in the low temperature range of 150-250 °C and the other in the high temperature range of 400-500 °C. These low and high NH₃-desorption peaks correspond to the weak and strong acid sites, respectively.²² In this figure, two of the three catalysts, SnO₂/ZY and SnO₂-K₂O/ZY, with the exception of pure SnO₂, exhibited a strong peak at a low temperature of around 70 °C and a weak shoulder peak around 160 °C. A significant point was the shift in the acid sites to low temperatures with the addition of the K component of the alkali metal. In our results, the ethanol-reforming reaction was further improved at low temperature and the activation point was shifted to a lower temperature in the SnO₂-K₂O/ZY catalyst. Various changes corresponding to the reduction of the SnO₂/SnO/Sn²³ components were

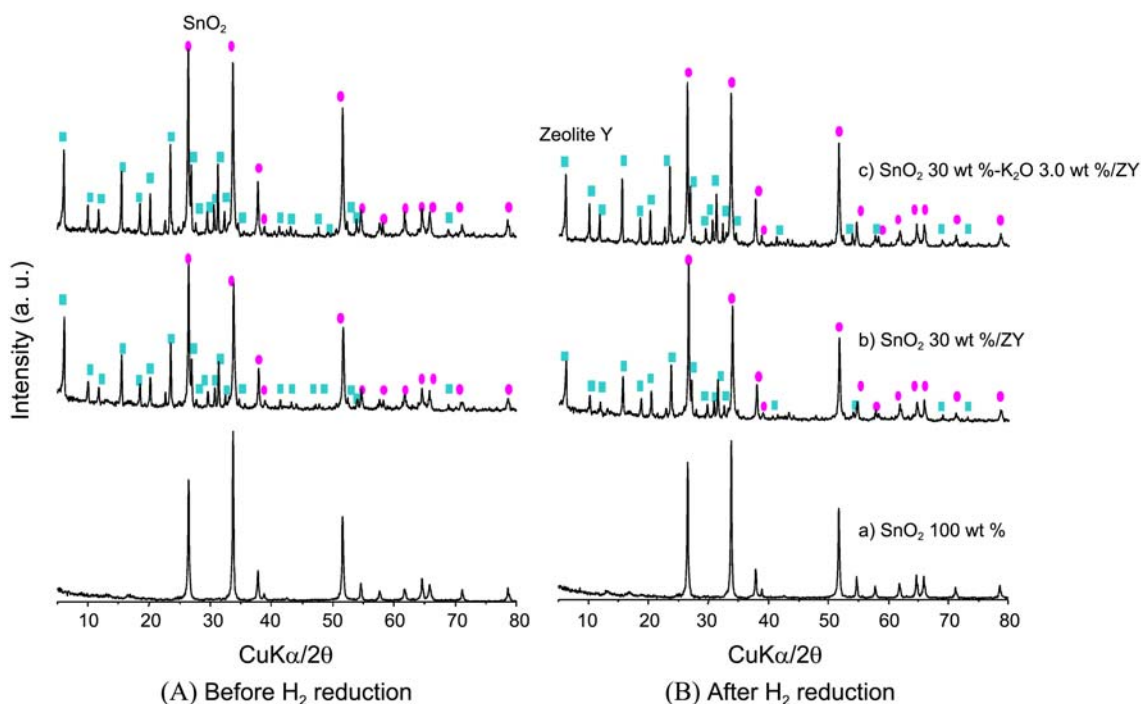


Figure 1. XRD patterns of the three catalysts, SnO₂ 100 wt %, SnO₂ 30 wt %/ZY, and SnO₂ 30 wt %-K₂O 3.0 wt %/ZY, before and after H₂ reduction.

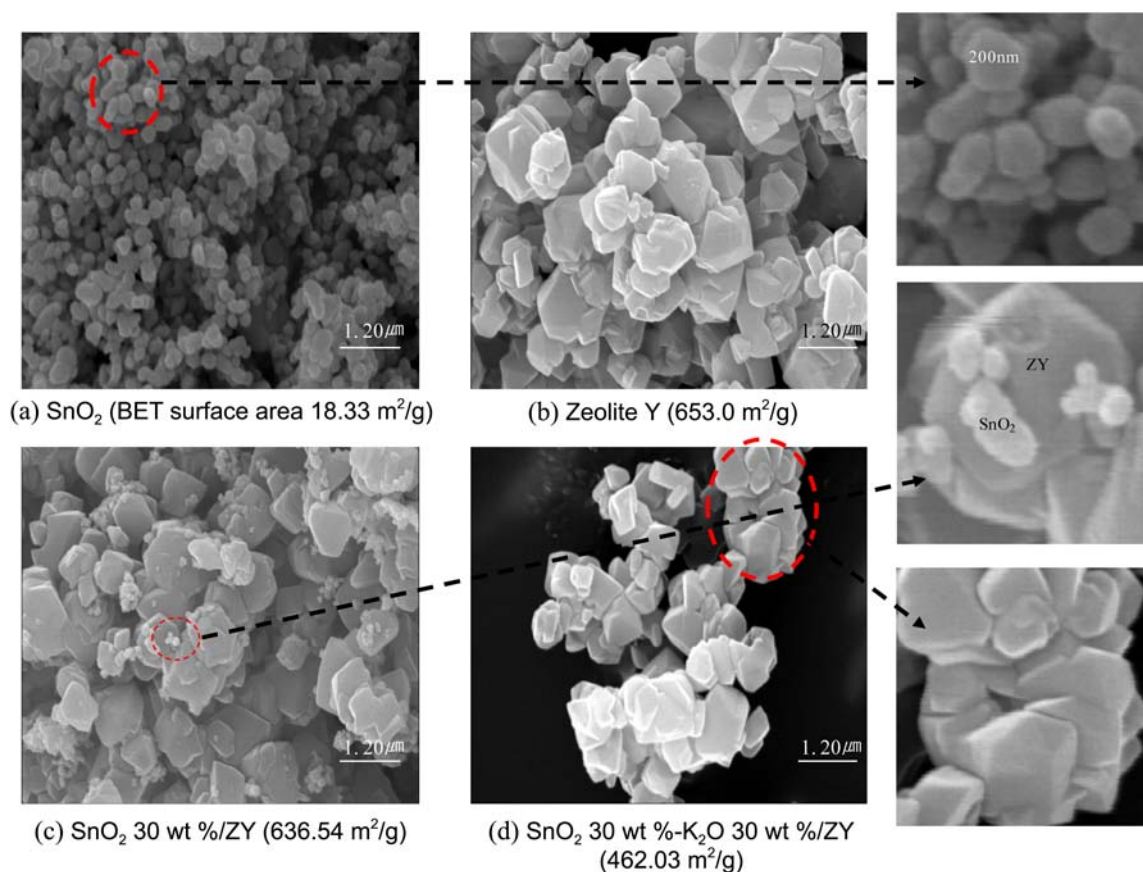


Figure 2. FESEM images of the four samples, SnO₂ 100 wt %, Zeolite Y, SnO₂ 30 wt %/Zeolite Y, and SnO₂ 30 wt %-K₂O 3.0 wt %/ZY, before and after H₂ reduction.

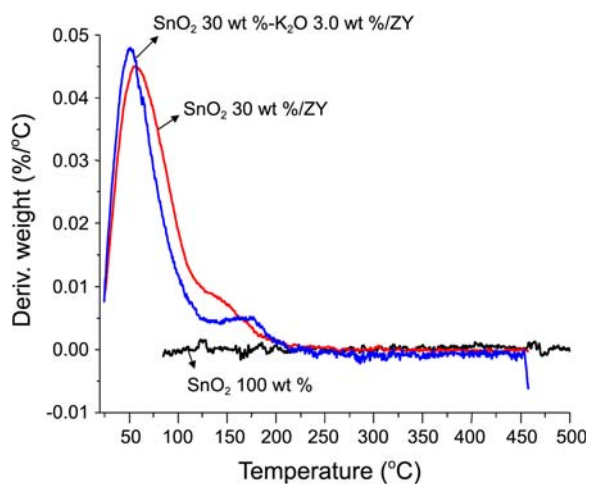


Figure 3. NH₃-TPD curves of the three catalysts: SnO₂ 100 wt %, SnO₂ 30 wt %/ZY, and SnO₂ 30 wt %-K₂O 3.0 wt %/ZY.

observed in the H₂-TPR profiles of the three catalysts shown in Figure 4. In general, the H₂-TPR results indicated that the peak area corresponds to the hydrogen uptake and that the peak at high temperatures corresponds to the catalytic reaction involved in the reduction mechanism. The reduction of the Sn⁴⁺ component exhibited in the SnO₂ catalysts at 500–680 °C was considered to be SnO₂→Sn. However, the reduction peak was separated into two types,

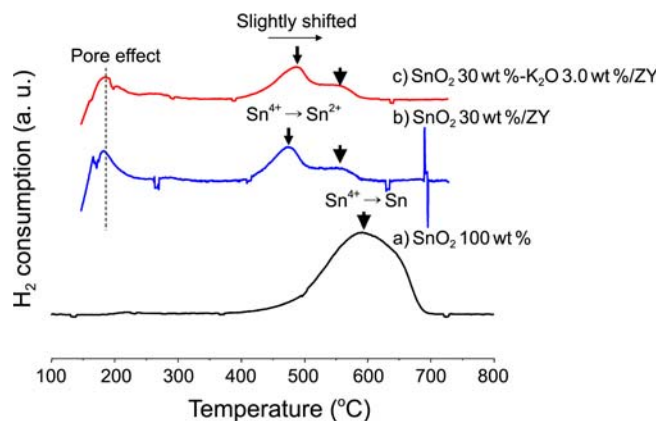


Figure 4. H₂-TPR curves of the three catalysts: SnO₂ 100 wt %, SnO₂ 30 wt %/ZY, and SnO₂ 30 wt %-K₂O 3.0 wt %/ZY.

SnO₂→SnO and SnO₂→Sn at 420–480 °C and 540–580 °C, respectively, and shifted to lower temperatures in the SnO₂-loaded Zeolite Y catalysts compared to that of pure SnO₂. Particularly with K addition, a slight shift toward a higher temperature was observed with SnO₂-K₂O/ZY. This indicates that the Sn species can be affected by the support property. Otherwise the peak due to the reduction of Al₂O₃ to Al was not seen above 700 °C, and a peak at around 170 °C was assigned to hydrogen uptake in internal pores of Zeolite Y.

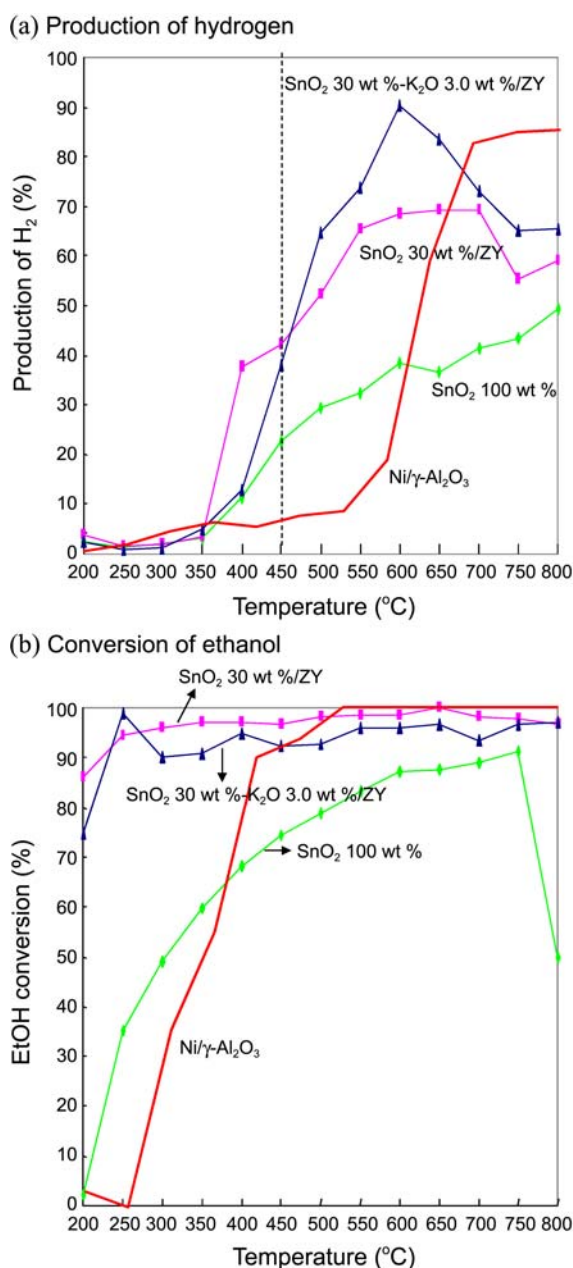


Figure 5. Ethanol conversion and H₂ production over the three catalysts: SnO₂ 100 wt %, SnO₂ 30 wt %/ZY, and SnO₂ 30 wt %-K₂O 3.0 wt %/ZY, according to the reaction temperature: A) H₂ production and B) ethanol conversion. Reaction conditions: catalyst weight 0.4 g; GHSV 12700/h; EtOH:H₂O = 1:1; time interval 50 °C.

Ethanol Steam-Reforming (ESR) Reaction over the Three Catalysts. ESR was carried out with 0.4 g of each of the three catalysts under the reaction conditions of temperature=200–800 °C, GHSV=12,700/h, and H₂O/EtOH=1.0. Figure 5 compares the time-on-stream activity of the three catalysts. In b), in which only the ethanol conversion is compared, the conversion over the SnO₂ 30 wt %-loaded catalysts, in contrast to that over the SnO₂ 100% catalyst, exceeded 90% from 250 °C, and this high performance was maintained to 800 °C. However, the ethanol conversion was increased over the SnO₂ 100% catalyst with increasing

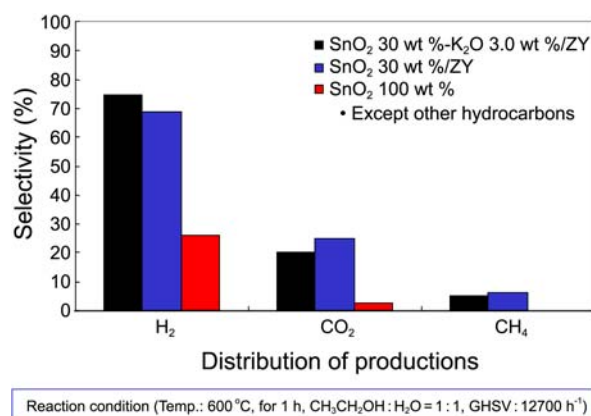


Figure 6. Production distribution during ESR according to the reaction temperature over the three catalysts. Reaction conditions: catalyst weight 0.4 g; GHSV 12700/h; EtOH:H₂O = 1:1; reaction temperature 600 °C; reaction time 1 h.

temperature up to 800 °C, above which it was remarkably decreased, which indicated catalytic deactivation. On the other hand, the hydrogen production gradually increased in the temperature range of 350 to 600 °C over all three catalysts. The hydrogen evolution was maximized over SnO₂ 30 wt %-K₂O 3.0 wt %/ZY at 89% at 600 °C, but then decreased to 70% as the temperature was further increased above 600 °C. This may have been caused by the methanation of carbon dioxide and carbon monoxide on the Al sites in the Zeolite Y support, which induced catalytic deactivation. However, the methanation effect was smaller over SnO₂ 30 wt %-K₂O 3.0 wt %/ZY than over the SnO₂ 30 wt %-loaded catalyst, due to the K-induced reduction in the acid sites. The Sn-loaded catalysts provided a significantly higher reforming reactivity than the conventional Ni/ γ -Al₂O₃ catalyst which added to compare, suggesting that the SnO₂ particles can be prevented from sintering with the support, which was further attributed to a synergy effect between Sn and K. Particularly, SnO₂-K₂O/Zeolite Y catalyst shows the best performance at a temperature of 500–700 °C, whereas increasing temperature is to increase the catalyst performance in the case of Ni/ γ -Al₂O₃. Eventually, ESR mechanism over SnO₂-K₂O/Zeolite Y catalyst is assumed to be different over the Ni/ γ -Al₂O₃ catalytic reaction.

Figure 6 shows the product distribution, relative to 100% ethanol conversion, over the three catalysts that were obtained from ESR at 600 °C after 1 h. The reactions were conducted under conditions of EtOH:H₂O = 1:1 and GHSV = 12,700 h⁻¹. The three species present in the product distribution, H₂, CO₂, and CH₄, were distributed according to the ratio of 27:3:0, 68:26:6, and 75:20:5 for SnO₂ 100 wt %, SnO₂ 30 wt %/Zeolite Y, and SnO₂ 30 wt %-K₂O 3.0 wt %/ZY catalysts, respectively. Significantly, the CO selectivity was near to zero percent over all three catalysts across the entire temperature range, and the CH₄ production was slightly increased. The presence of CO degrades the active catalyst due to catalyst poisoning by CO molecules.²⁴ Therefore, our results demonstrated the synergistic effect of the introduction of Sn, K, and Zeolite Y support on the catalytic

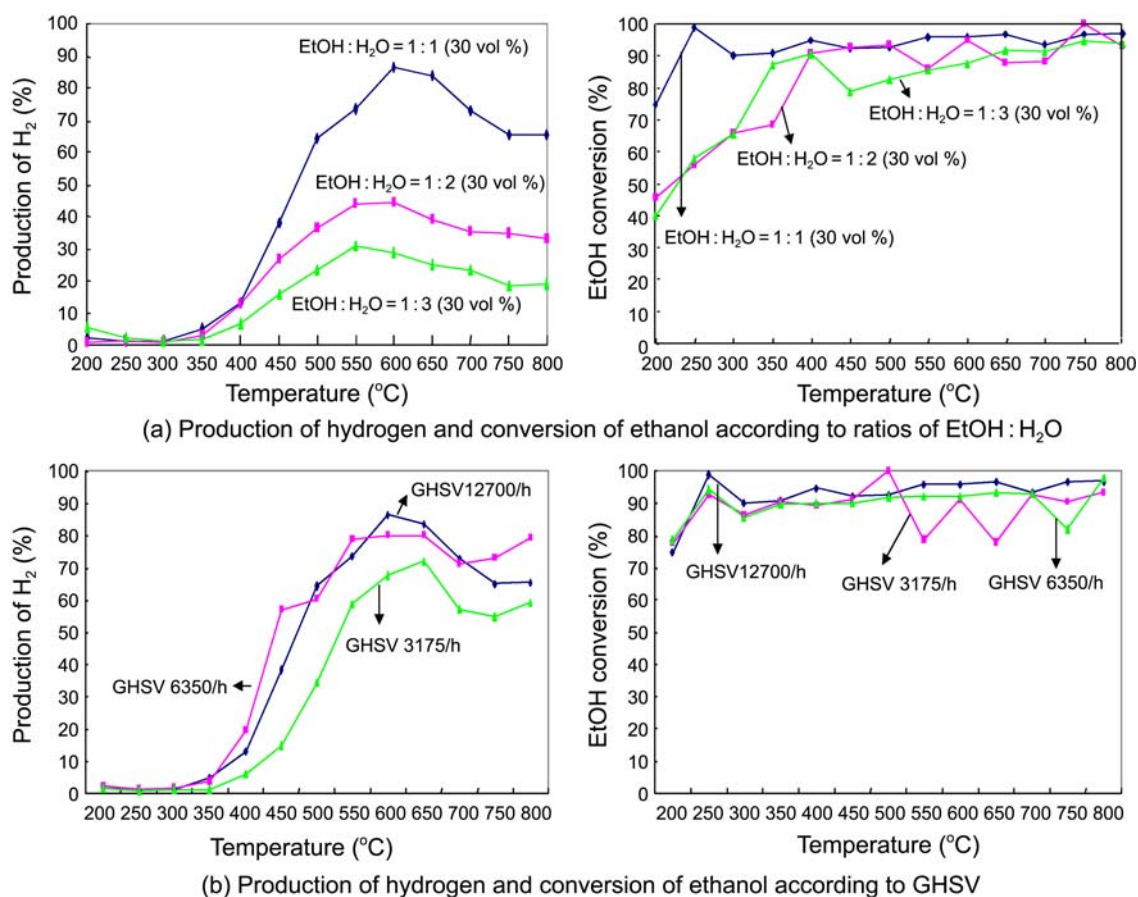


Figure 7. Catalytic performances for the ESR reaction over the SnO₂ 30 wt %-K₂O 3.0 wt %/ZY catalyst with various ethanol/steam concentrations and GHSV values. Reaction conditions: catalyst weight 0.4 g; GHSV 3175, 6350, and 12700/h; EtOH:H₂O = 1:1, 1:2, and 1:3; reaction time 1 h; time interval 50 °C.

performance, along with the depressing sintering phenomenon and consequent reduction in catalytic deactivation. Figures 7(a) and 7(b) show the catalytic performances for the ESR reaction over the SnO₂ 30 wt %-K₂O 3.0 wt %/ZY catalyst with various ethanol/steam concentrations, diluted in argon gas of 30 vol %, and at various GHSV values. In Figure 7(a), the optimal conditions corresponded to an EtOH:H₂O ratio of 1:1 and 89% of the hydrogen was emitted at 600 °C, with an ethanol conversion of 97%. However, the ethanol conversion was slightly decreased at higher water concentrations. Otherwise, the H₂ production was positively correlated with GHSV from the reaction temperature of 350 °C with an ethanol conversion exceeding 90% over the entire GHSV range, as shown in Figure 7(b). The efficiency of the ethanol conversion and hydrogen production were both increased with increasing GHSV over the complete temperature range. Therefore, the optimal reaction conditions according to the active response for the production of H₂ over the SnO₂ 30 wt %-K₂O 3.0 wt %/ZY catalyst were a GHSV of 12,700 h⁻¹, a ethanol steam concentration of 1:1 (30 vol %), and a reaction temperature of 600 °C.

Characteristics of the Three Catalysts After Ethanol Reforming. Figure 8 compares the XRD patterns of the three catalysts after 10 h of the ESR reaction at 600 °C for the SnO₂ 30 wt %/ZY and SnO₂ 30 wt %-K₂O 3.0 wt %/ZY

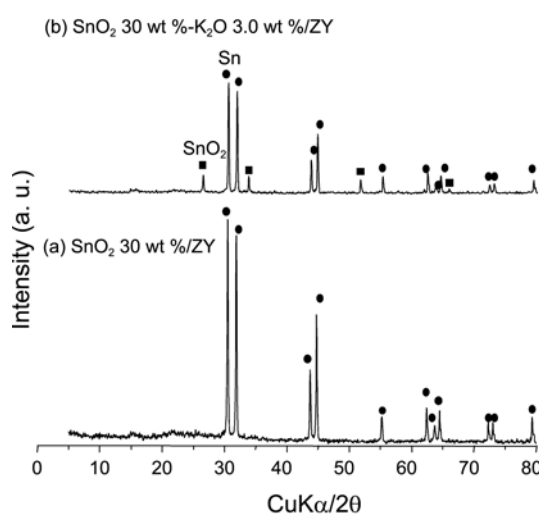


Figure 8. Comparison of XRD patterns for the two catalysts, SnO₂ 30 wt %/ZY and SnO₂ 30 wt %-K₂O 3.0 wt %/ZY, before and after reaction.

catalysts. Surprisingly, the Zeolite Y skeletal structure disappeared after the reaction, with only the Sn species remaining in both catalysts. The diffraction lines of the Sn metal phase²⁵ at 2θ angles of 31, 32, 43, 44, 56, 62, 63, 64, 73, 74, and 79° were clearly expressed after the reaction in both

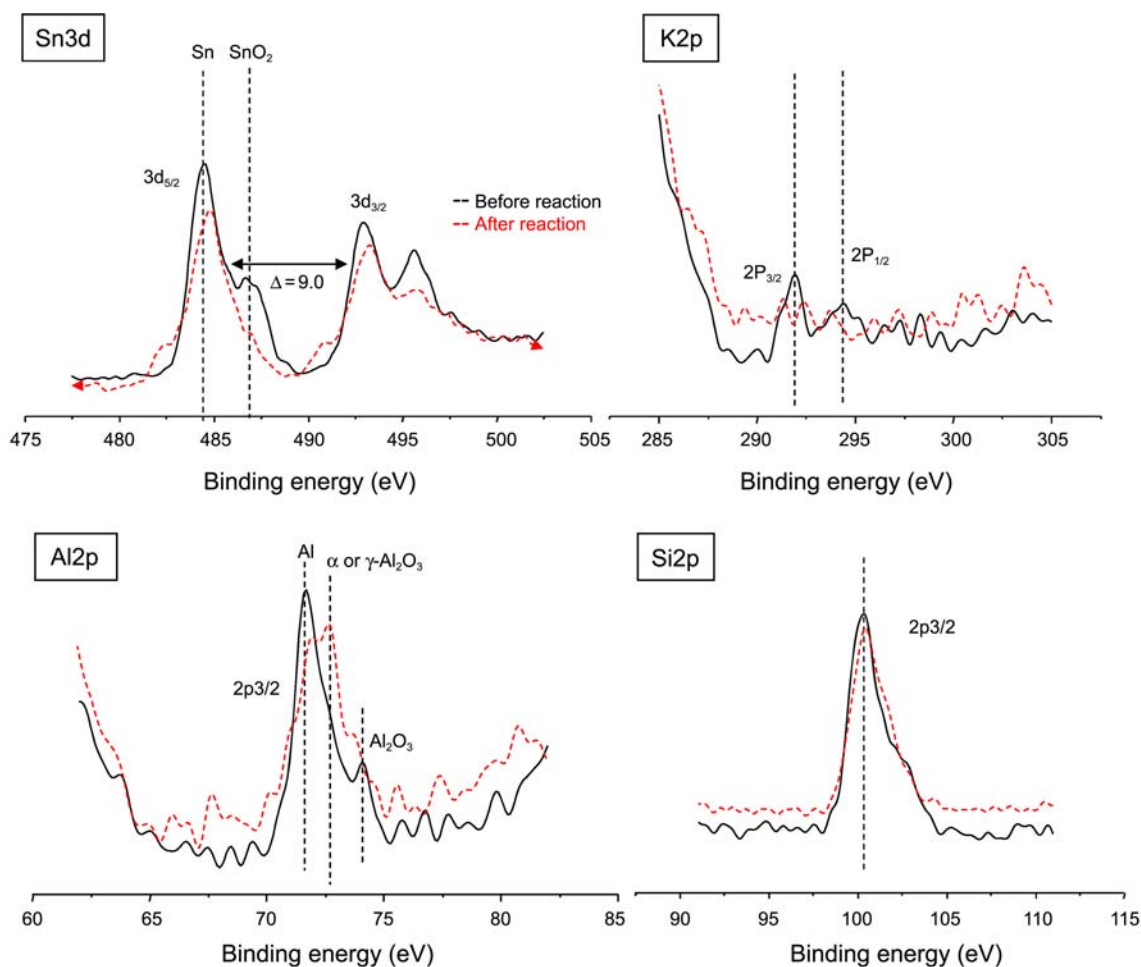


Figure 9. Comparison of XPS curves for Sn3d, K2p, Al2p, and Si2p orbitals of the SnO₂ 30 wt %-K₂O 3.0 wt %/ZY catalyst, before and after reaction.

catalysts, and additionally the peaks assigned to SnO₂ were smaller than those before the reaction in the SnO₂ 30 wt %-K₂O 3.0 wt %/ZY catalyst. This indicated that the SnO₂ components acted as active sites in the ESR reaction, and the peak decrease after the reaction automatically implies a comparison with that before the reaction for the SnO₂ 30 wt %-K₂O 3.0 wt %/ZY catalyst. Figure 9 presents the typical survey and high-resolution spectra obtained from the quantitative XPS analyses of the SnO₂ 30 wt %-K₂O 3.0 wt %/ZY catalyst. The survey spectra of the particles contained the Sn3d, K2p, Al2p, and Si2p peaks, which were analyzed based on an XPS handbook.²⁶ The Al2p_{3/2} spin-orbital photoelectron in the Al component in Zeolite Y was located at binding energies of 72.0 eV and 74.5 eV before the reaction, which corresponded to α - or γ -Al₂O₃ and Al oxides, respectively. However, these binding energies were further separated into three types at 72.5 eV, 73.0, and 74.0 eV for 2p_{3/2} at the maximum points after the reaction, which were assigned to α - or γ -Al₂O₃, dense sapphire-type Al₂O₃, and Al oxides, respectively. This means that the Al components were transferred to dense sapphire-type Al₂O₃ during high-temperature ethanol reforming. The Si2p_{3/2} orbital at 100.5 eV, which was assigned to SiO₂ in Zeolite Y, was unchanged except for slightly peak broadening after the

reaction. On the other hand, the Sn3d region in the spectra of Sn oxide was decomposed into two contributions, which were assigned to Sn3d_{5/2} and Sn3d_{3/2} at 484.0 (for Sn metal) ~486.5 (for SnO₂) and 493.0-496.0 eV, respectively.²⁶ The Sn components were transferred to the more reduced form of SnO₂→Sn, with the Sn metal portion at 484.0 eV comprising more than 90% after the ethanol reforming reaction. This result indicated that the Sn oxides in the catalyst were reduced to lower oxidation states after the ethanol reforming by H₂ gas or other hydrocarbon intermediates. In addition, the same phenomenon occurred before the reaction for K2p_{3/2} and K2p_{1/2} at binding energies of 292.0 and 294.0 eV, which were assigned to K⁺ in this study.²⁶ However, the peak intensities were largely decreased with no change of peak position after the reaction, and, furthermore, the other small peak of K2p_{3/2} was seen at a higher binding energy of 292.5 eV, which revealed the presence of another K oxidized state. These results indicated that the Sn ions were reduced after the ethanol reforming and, consequently, confirmed their involvement in the oxidation of ethanol or other hydrocarbons that were evolved during the ethanol-reforming reaction to afford the production of CO₂ molecules. Otherwise, we expected the K component to act as a reducing agent and thus depress the hydrocarbon production during the ethanol

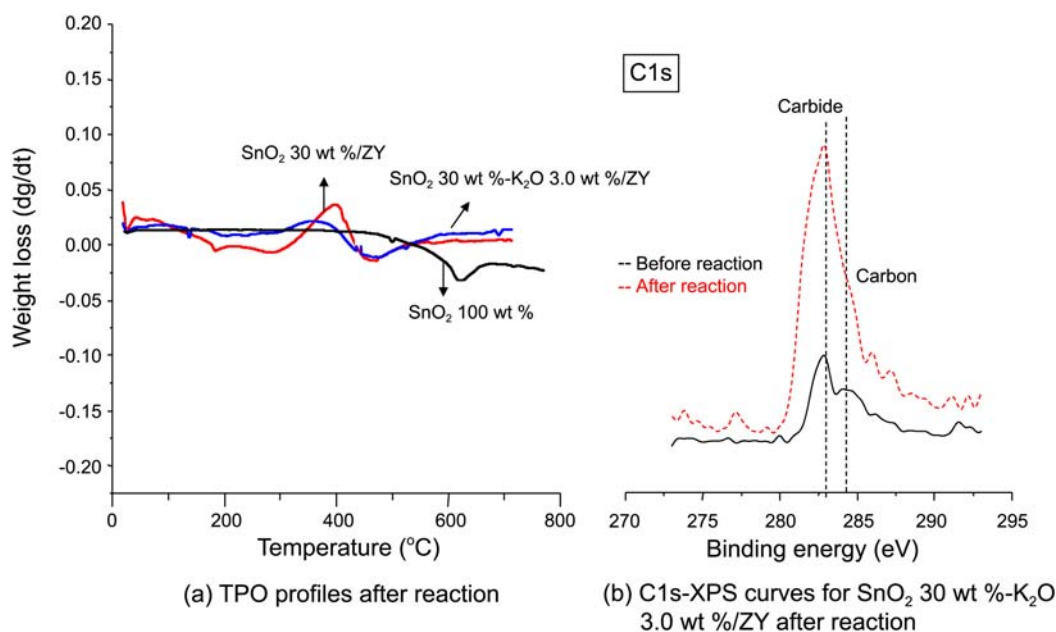


Figure 10. TPO profiles of SnO₂ 100 wt %, SnO₂ 30 wt %/ZY and SnO₂ 30 wt %-K₂O 3.0 wt %/ZY catalysts, and XPS curve of C1s orbital of the SnO₂ 30 wt %-K₂O 3.0 wt %/ZY catalyst before and after reaction. Reaction conditions: catalyst weight 0.4 g; GHSV 12700/h; EtOH:H₂O = 1:1; reaction temperature 600 °C, reaction time 10 h.

reforming reaction. To determine the amount of carbon deposited on the catalysts, we carried out TPO measurements (A) and C1s XPS analysis (B), as shown in Figure 10. The deposited amount (peak area) and species of carbons (decomposed temperature) were closely related to the catalytic deactivation. Generally, the extent of catalytic deactivation is reduced with a smaller amount of deposited carbon. The carbon desorption curve for the SnO₂ 100% catalyst was extremely small and broad up to 600 °C, after which combustion occurred. When the Sn-only component was exposed to the outside surface of the Zeolite Y, the deposited carbons underwent greater oxidation at high temperatures compared to the sample with the Sn-K component, indicating the deposition of heavy carbons. Similar amounts of carbon were deposited in the SnO₂ 30 wt %-K₂O 3.0 wt %/Zeolite Y catalyst, but the peak position was shifted to a lower temperature, and the amount was decreased. We therefore concluded that the co-existence of Sn and K helped to retain the structural stability and avoid their conglomeration in the ESR reaction, which is in agreement with the better stability demonstrated by the SnO₂ 30 wt %-K₂O 3.0 wt %/ZY catalyst compared with SnO₂ 30 wt %/ZY. On the other hand, although one C1s orbital is generally seen at 284.5 eV for bulky carbons,²⁶ the peak in this study could be split into two peaks at around 283.0 and 284.0 eV due to the mixture of carbide and carbon species in the coke deposition over the SnO₂ 30 wt %-K₂O 3.0 wt %/ZY catalyst. The peak before the reaction was small, but strengthened after the reaction, and these data were in agreement with the TPO profiles.

Investigation of the Catalytic Lifetime of the SnO₂ 30 wt %-K₂O 3.0 wt %/ZY Catalyst. Finally, the catalytic deactivation was tested for the SnO₂ 30 wt %-K₂O 3.0 wt %/

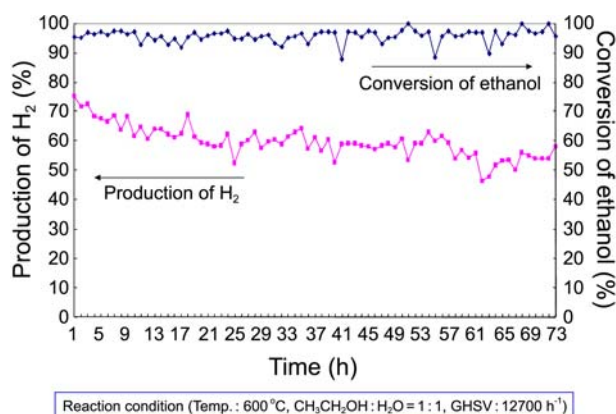


Figure 11. Test of catalytic deactivation over SnO₂ 30 wt %-K₂O 3.0 wt %/ZY catalyst. Reaction conditions: catalyst weight 0.4 g; GHSV 12700/h; EtOH:H₂O = 1:1; reaction temperature 600 °C, reaction time 73 h.

ZY catalyst, and the results are shown in Figure 11. Dramatically, the H₂ production was expressed in the range of 50–75% with an ethanol conversion of 90–100%. This result is very similar with the previously reported H₂ production of 70% at 600 °C with the high-cost Pd/Ni/Zeolite Y component.¹⁸ Although the catalytic deactivation was retarded until 53 h over the former, rapid deactivation subsequently occurred, indicating that the initial catalyst deactivation may have resulted from a combination of steam-induced nickel sintering and carbon deposition. However, the apparent deactivation rate was far lower for the Sn-promoted catalyst and its higher ethanol conversion was maintained for up to 73 h. Thus, the improved stability at the slower deactivation rate achieved with the Sn-K sample could not be unequivocally attributed to carbon formation.

Conclusion

The two key study findings are the effects of the Sn and K presence on the variation in H₂ production and on the retardation of the catalytic deactivation. On the basis of the performance results and a variety of physical measurements, we proposed that the Sn component played a role in the oxidation of the feed gases during ethanol reforming, resulted in the production of CO₂. Otherwise, the addition of the K component depressed the presence of CH₄ or other hydrocarbon intermediates. The simultaneous addition of Sn and K may have induced a synergy effect that increased the ethanol conversion and H₂ production over the SnO₂ 30 wt %-K₂O 3.0 wt %/ZY catalyst to 100% and 89%, respectively. This high performance was maintained for up to 73 h. The operational conditions, as identified by a parametric study, were a reaction temperature of 600 °C, GHSV of 12,700 h⁻¹, and feed ratio of ethanol:H₂O of 1:1. This result seems to be attributable to the following; based on the results of H₂-TPR and NH₃-TPD, the reduction of Sn oxides generates on SnO₂-K₂O/ZY catalyst at low temperatures compared to conventional Ni/γ-Al₂O₃ catalysts, eventually the compatible change between Sn⁴ and Sn⁰ easily occurs. Moreover, differently the Ni/γ-Al₂O₃ catalyst has the strong acidity which induced by the existing Al, the SnO₂-K₂O/ZY catalyst expresses a weak acid resulted that the condensations of ethanol are difficult and formed less coke formation, and eventually the higher activity over SnO₂-K₂O/ZY catalyst is maintained.

Acknowledgments. This work was supported by the New & Renewable Energy of the Korea Institute of Energy Technology Evaluation and Planning (KETEP) grant funded by the Korea Government Ministry of Knowledge Economy (No. 2010T100100622).

References

1. Koh, A. C. W.; Chen, L.; Leong, W.; Ang, T. P.; Johnson, B. F. G.; Khimyak, T.; Lin, J. *Inter. J. Hydrogen Energy* **2009**, *34*, 56913.
2. Busca, G.; Costantino, U.; Montanari, T.; Ramis, G.; Resini, C.; Sisani, M. *Inter. J. Hydrogen Energy* **2010**, *35*, 5356.
3. Campos-Skrobot, F. C.; Rizzo-Domingues, R. C. P.; Fernandes-Machado, N. R. C.; Cantão, M. P. *J. Power Sources* **2008**, *183*, 713.
4. Srisiriwat, N.; Therdthianwong, S.; Therdthianwong, A. *Inter. J. Hydrogen Energy* **2009**, *34*, 2224.
5. Sánchez-Sánchez, M. C.; Navarro, R. M.; Fierro, J. L. G. *Catal. Today* **2007**, *129*, 336.
6. Goula, M. A.; Kontou, S. K.; Tsiakaras, P. E. *Appl. Catal. B* **2004**, *49*, 135.
7. Ribeiro, R. U.; Liberatori, J. W. C.; Winnishofer, H.; Bueno, J. M. C.; Zanchet, D. *Appl. Catal. B* **2009**, *91*, 670.
8. Al-Fatish, A. S. A.; Ibrahim, A. A.; Fakeeha, A. H.; Soliman, M. A.; Siddiqui, M. R. H.; Abasaed, A. E. *Appl. Catal. A* **2009**, *364*, 150.
9. Koo, Y.; Roh, H. S.; Seo, Y. T.; Seo, D. J.; Yoon, Y. L.; Park, S. B. *Appl. Catal. A* **2008**, *340*, 183.
10. Soybal-Baltacıoğlu, F.; Aksoylu, A. E.; Önsan, Z. I. *Catal. Today* **2008**, *138*, 183.
11. Ciambelli, P.; Palma, V.; Ruggiero, A. *Appl. Catal. B* **2010**, *96*, 190.
12. Jacobs, G.; Keogh, R. A.; Davis, B. H. *J. Catal.* **2007**, *245*, 326.
13. de la Peña O'Shea, V. A.; Nafria, R.; Ramírez de la Piscina, P.; Homs, N. *Inter. J. Hydrogen Energy* **2008**, *33*, 3601.
14. Zhang, B.; Tang, X.; Li, Y.; Xu, Y.; Shen, W. *Inter. J. Hydro Energy* **2007**, *32*, 2367.
15. Choi, S. H.; Kim, J. S.; Yoon, Y. S. *Electrochimica Acta* **2004**, *50*, 547.
16. Jeon, Y. A.; No, K. S.; Choi, S. H.; Ahn, J. P.; Yoon, Y. S. *Electrochimica Acta* **2004**, *50*, 907.
17. Yang, J.; Hidajat, K.; Kawi, S. *Mater. Letters* **2008**, *62*, 1441.
18. Kwak, B. S.; Kim, J.; Kang, M. *Inter. J. Hydro Energy* **2010**, *35*, 11829.
19. Mukhopadhyay, K.; Chaudhari, R. V. *J. Catal.* **2003**, *213*, 73.
20. Zhang, D.; Song, F.; Su, H.; Han, J.; Xu, J. *Sens. Actuators B* **2010**, *145*, 39.
21. Li, G.; Pickup, P. G. *J. Power Sources* **2007**, *173*, 121.
22. Kovalenko, V. V.; Zhukova, A. A.; Romyantseva, M. N.; Gaskov, A. M.; Yushchenko, V. V.; Ivanova, I. I.; Pagnier, T. *Sens. Actuators B* **2007**, *126*, 51.
23. D'Arino, M.; Pinna, F.; Strukul, G. *Appl. Catal. B* **2004**, *53*, 61.
24. Zhu, H.; Qin, Z.; Shan, W.; Shen, W.; Wang, J. *J. Catal.* **2004**, *225*, 267.
25. Takemoto, T.; Joo, Y. J. *Mater. Lett.* **2002**, *56*, 793.
26. Moulder, J. F.; Stickle, W. F.; Sobol, P. E.; Bomben, K. D. *Handbook of X-ray Photoelectron Spectroscopy Perkin-Elmer Corporation* **1992**.